

# Simultaneous Detection of Loop-Closures and Changed Objects

Tanaka Kanji Yamaguchi Kousuke Sugimoto Takuma

## ABSTRACT

*Loop-closure detection (LCD) in large non-stationary environments remains an important challenge in robotic visual simultaneous localization and mapping (vSLAM). To reduce computational and perceptual complexity, it is helpful if a vSLAM system has the ability to perform image change detection (ICD). Unlike previous applications of ICD, time-critical vSLAM applications cannot assume an offline background modeling stage, or rely on maintenance-intensive background models. To address this issue, we introduce a novel maintenance-free ICD framework that requires no background modeling. Specifically, we demonstrate that LCD can be reused as the main process for ICD with minimal extra cost. Based on these concepts, we develop a novel vSLAM component that enables simultaneous LCD and ICD. ICD experiments based on challenging cross-season LCD scenarios validate the efficacy of the proposed method.*

## I. INTRODUCTION

Recent progress in robotic visual simultaneous localization and mapping (vSLAM) has led to the development of various practical vSLAM systems (e.g., ORB-SLAM) that are able to map large non-stationary environments via robot-centric monocular vision. Loop-closure detection (LCD), which is the problem of detecting loop-closure events, is crucial for addressing the inherently accumulative self-localization errors in vSLAM [1]. However, LCD in large non-stationary environments (e.g., cross-season LCD [2]) remains a significant challenge. A major source of difficulty is the large number of possible changes between live images and a map (e.g., car parking, furniture movement), which grows combinatorially relative to map size.

To reduce computational and perceptual complexity, it is helpful if a vSLAM system has the ability to detect changed objects. The detected changes can then be used to inspect and update the corresponding parts of a map.

Detecting changes in a query live image relative to a pre-trained background (or reference) model is a fundamental problem in computer vision called image change detection (ICD) [3] that has been studied in many different contexts including remote sensing [4] and surveillance [5].

In these classical contexts, the problem is typically formulated as a two-stage offline-online process, where the online process aims to detect changes in a live image, relative to an offline pre-trained background model. However, such separate offline-online stages are not applicable to vSLAM, which has no offline stage. Furthermore, it is impractical to maintain a background model online within the real-time budget allowed for vSLAM.

To address the above issues, we introduce a novel maintenance-free ICD algorithm that requires no background modeling stage. Specifically, we propose reusing the latest map database and LCD engine, which are continually maintained and kept up-to-date by vSLAM, in place of a maintenance-intensive background model and detector engine, respectively. This idea is supported by the recent findings in the field of multi-experience localization [6] that errors in self-localization (i.e., LCD) can be viewed as a good indicator of inconsistency (i.e., changes) between encountered conditions and a map. This approach has two main merits. First, we can introduce such an ICD system with very little additional cost. Second, we can directly detect degradation of map quality (i.e., the need for map updating) in terms of LCD errors.

In this paper, we present a novel vSLAM component, called “LCD-ICD” that enables the simultaneous detection of loop-closures and changed objects. LCD-based ICD is motivated by our previous work [7], but that work focused on a pose-tracking scenario, rather than the global localization (i.e., LCD) scenario addressed in this paper. Note that such a simultaneous formulation is required because localizing changed objects in the world requires a reliable estimate of robot pose (i.e., LCD). We employ the bag-of-local-features (BoLF) image representation because it is a standardized representation for state-of-the-art LCD systems [8] and an effective image model for ICD [9]. We adopt a generic LCD formulation that models an LCD system as a ranking function. We also derive unsupervised rank fusion techniques from the field of multi-media information retrieval [10] to fuse different ranking results from different local query features into a pixel-wise likelihood-of-change (LoC) measure. Consequently, our ICD system is maintenance-free, requiring no background model or detector engine. It is also agnostic to the choice of LCD system. We implemented the proposed ICD framework and evaluated the feasibility of simultaneous LCD and ICD in a practical challenging cross-season LCD scenario [11]. The experimental results demonstrate that the proposed LCD-ICD method is comparable to or superior to standard ICD methods, despite the fact that the proposed system is maintenance-free.

Our work has been supported in part by JSPS KAKENHI Grant-in-Aid for Scientific Research (C) 26330297, and (C) 17K00361.

K. Tanaka is with Faculty of Engineering of Graduate School of Engineering, University of Fukui. K. Yamaguchi and T. Sugimoto are with Graduate School of Engineering, University of Fukui, Japan. [tnkknj@u-fukui.ac.jp](mailto:tnkknj@u-fukui.ac.jp)

## II. LCD FRAMEWORK

We follow a standard LCD framework consisting of three distinct stages. At each time step, (1) the current live image is converted into a BoLF representation (Section II-A) and (2) a similarity search over a database of reference images is performed to find the nearest neighbor reference images (Section II-B). Finally, (3) the map is updated by incorporating the latest live image for future LCD tasks (Section II-C). Each of these stages is detailed in the following subsections.

### A. BoLF Representation

Converting a live image into a BoLF representation is an important stage of the LCD process. First, semantically coherent object proposal regions (OPRs) representing scene parts are extracted from an image. Next, each OPR is converted into a visual feature. These two processes are detailed below.

For OPR extraction, we introduce supervised and unsupervised object proposal methods that extract OPRs in the form of bounding boxes (BBs). The supervised proposal method from [12] is employed to extract 1-11 OPRs per image (Fig. 1b). The unsupervised proposal method generates five additional bounding boxes  $[w/3, 2w/3] \times [h/3, 2h/3]$ ,  $[0, 2w/3] \times [0, 2h/3]$ ,  $[w/3, w] \times [0, 2h/3]$ ,  $[0, 2w/3] \times [h/3, h]$ , and  $[w/3, w] \times [h/3, h]$  for a  $w \times h$  image. Therefore, we extract a total of 6-16 OPRs per image.

For feature extraction, we use the intermediate layer of an unsupervised AE as a feature extractor. This design choice was motivated by the recent success of AEs in LCD applications [13]. Importantly, it can be trained in an unsupervised manner, requiring only unlabeled images from the target environments. For these properties, future widespread use of such AE-based LCD systems are expected. The authors of [13] trained a domain-specific AE using training images that were collected from the target environment. In contrast, we pretrain a generic AE using an independent train image set, with the goal of performing domain-generic LCD. Our AE architecture uses a layer structure of 128-64-32-16-16-32-64-128 nodes, and is trained on a collection of reference images. Every image is resized to  $256 \times 256$  pixels prior to inputting it into the AE.

### B. Similarity Search

The similarity search stage aims to find similar images to a query image. The BoLFs in all reference images are ranked in descending order of similarity. In this work, the L2 norm was used as a similarity measure.

### C. Map Updating

The map updating stage aims to insert the current live image into the map database for future LCD. Each local feature in the live image is used as an index into the map database.

## III. ICD BASED ON LCD

We now introduce our ICD component as a function of LCD. In this section, we begin by assuming the availability of a “ground-truth (GT)” reference image as the reference image whose viewpoint is closest to the current viewpoint. This assumption will be relaxed in the following section. Fig. 1 illustrates the formulation of our LoC prediction problem.

The majority of works on BoLF based LCD models use LCD as a ranking function. Let us assume that a total of  $n$  images are contained in a map database  $D = \{I_i\}_{i=1}^n$ . Each image  $I_i$  has a set of local features  $\{x_{ij}\}_{j=1}^{d_i}$ , where  $d_i$  is the number of local features. Given a query image, a similarity search (section II-B) is performed using each local feature as a query. Then, for each local feature in the query image, a ranked list of reference images in the descending order of similarity is returned.

In our approach, this LCD system is reused to estimate the LoC of a given query image (Fig. 1a). Given the local features  $\{x_{ij}\}_{j=1}^{d_i}$  of multiple overlapping OPRs in a query image, we retrieve a map and obtain  $d_i$  rank lists. Then, the LoC of each  $j$ -th OPR is measured based on the rank values  $\{\{r_{ijk}\}_{k=1}^{d_i}\}_{j=1}^{d_i}$  (ascending order of similarity) of the  $k$ -th OPR in the GT reference image within the  $j$ -th ranked list.

We compute the anomaly score of the  $j$ -th OPR in the  $i$ -th query image as the minimum of the related reference OPRs:

$$r_{ij} = \min_k r_{ijk}. \quad (1)$$

Now we will characterize LoC measures for the LCD method (Fig. 1b). As mentioned above, rank values are obtained for each  $j$ -th OPR in the  $i$ -th query image, in the form of rank values of GT reference images. Therefore, it is natural to apply a pooling technique to aggregate these values (i.e., OPR-level LoC values) into a pixel-wise LoC value.

The rank aggregation problem was explored in the context of part-based self-localization in our previous study [14]. The method used in this study is based on our previous method with a few key modifications: First, our previous study aimed at image-level ranking, whereas this study aims to obtain pixel-level rank values. Second, the previous method took non-overlapping query subimages (from color-based segmentation) as inputs, whereas the current method takes overlapping query subimages (unsupervised/supervised OPRs) with *variable* amounts of overlap per pixel.

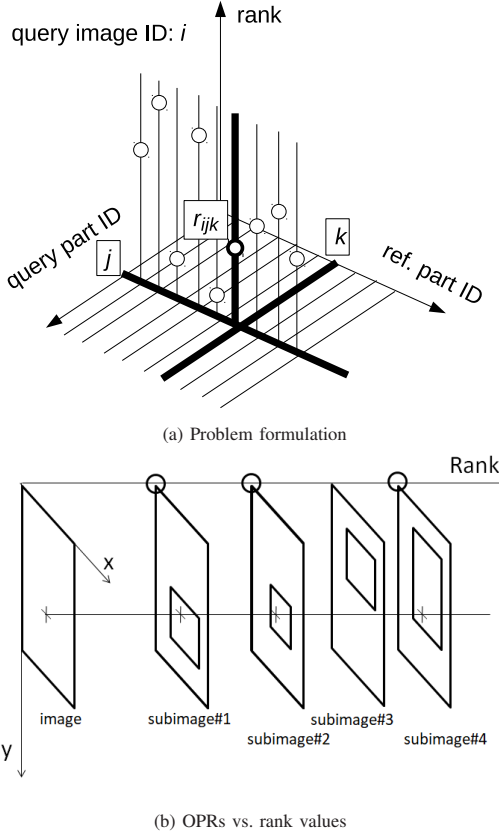


Fig. 1. LoC prediction. (a) Given an  $i$ -th query image, we perform VPR for each  $j$ -th scene part (OPR) in the query image to obtain a rank value  $r_{ijk}$  for each  $k$ -th OPR in the ground-truth (GT) reference image. (b) To compute a pixel-wise LoC map, the bounding boxes and rank values of the OPRs are translated into a pixel-wise LoC map, by aggregating the rank values of the OPRs that belong to each pixel of interest (+).

To address this issue, we must perform the novel task of pixel-wise rank fusion [7]. Formally, we adopt the recently presented extension of *variable* length rank lists for MMR [15], and fuse per-pixel ranking results as follows:

$$r_i[p] = |J[p]| / \left( \sum_{j \in J[p]} r_{ij}[p]^{-1} \right), \quad (2)$$

where  $J[p]$  is the set of identifiers of OPRs belonging to pixel  $p$ .

#### IV. SIMULTANEOUS LCD AND ICD

We now consider a more practical scenario in which GT references are not available. Instead, a collection of  $Y$  viewpoint hypotheses are provided by the similarity search of LCD (section II-B).

In our experimental system, the similarity search of LCD is based on the naive Bayes nearest neighbor (NBNN) similarity metric, which was proven to be effective in our previous study [16]. Given a query image BoLF  $f_i$  and a collection of reference image BoLFs  $\{f_{i'}^j\}$ , the problem of finding the nearest neighbor reference image  $j$  to a query image is defined as follows:

$$j = \arg \min_j \frac{1}{n_i} \sum_i \min_{i'} |f_i - f_{i'}^j|, \quad (3)$$

where  $n_i$  is the number of local features in the  $i$ -th image.

We consider the  $Y$  top-ranked viewpoint hypotheses (e.g.,  $Y = 10$ ) top-ranked from the similarity search and aggregate their LoC images into a single final LoC image.

For aggregation, we consider the nature of the proposed LCD-ICD system. Incorrect viewpoint hypotheses represent large LCD errors and cause an increase in the LoC value at every pixel in the LoC image. In other words, the LoC value at a pixel is much higher for incorrect viewpoint hypotheses than it is for correct viewpoint hypotheses. To filter out unreliable large LoC values, we perform pixel-wise minimum pooling to aggregate LoC image hypotheses in the form of  $r_i[p] = \min_h r_i[p][h]$ , where  $r_i[p][h]$  is the ranking result at pixel  $p$  for the  $h$ -th viewpoint hypothesis.

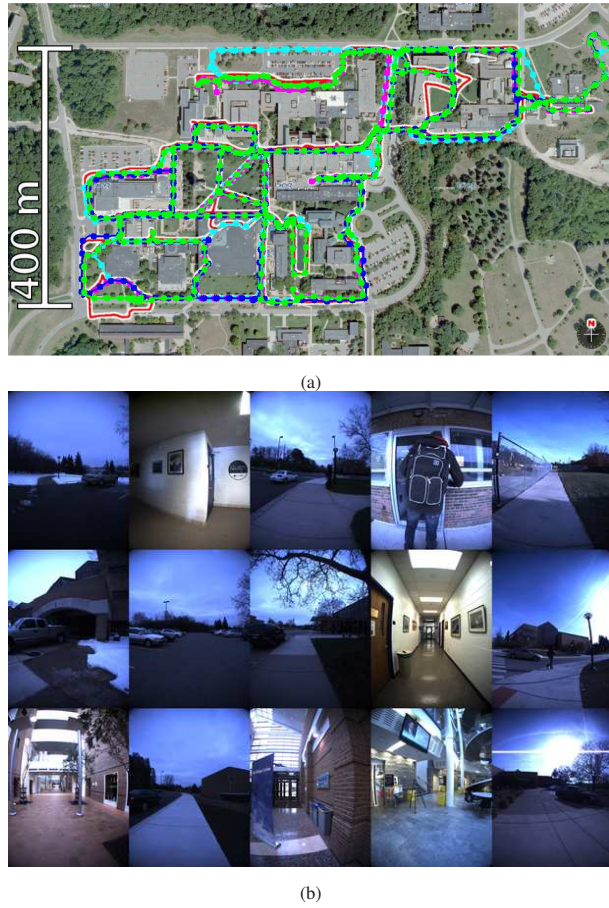


Fig. 2. Experimental environment, (a) vehicle trajectories and (b) changing objects.

## V. EXPERIMENTS

We evaluated the proposed ICD framework on a challenging cross-season LCD scenario.

### A. Settings

We used a public dataset, North Campus long-term (NCLT) dataset for our experiments [11]. The NCLT dataset is a large-scale, long-term autonomy dataset for robotics research that was collected at the University of Michigan’s North Campus by a Segway vehicle platform. The data we used in this study includes view image sequences along the vehicle trajectories acquired by the front facing camera of the Ladybug3 platform (Fig. 2). From the perspective of ICD benchmarking, the NCLT dataset has desirable properties. It includes various types of changing images such as cars, pedestrians, building construction, construction machines, posters, tables and whiteboards with wheels, from seamless indoor and outdoor navigations of the Segway vehicle. Additionally, it has recently gained significant popularity as a benchmark in the SLAM community [17].

In this study, we used four datasets labeled “2012/1/22”, “2012/3/31”, “2012/8/4”, and “2012/11/17” (denoted WI, SP, SU, and AU, respectively) collected from four different seasons. We annotated 986 different changing objects with bounding boxes in total. The annotations are found in all 12 possible pairings of query and reference seasons. The image size is  $1232 \times 1616$ . Additionally, we prepared a collection of 1,973 random destructor images, that are independent of the 986 annotated images and do not contain changing objects. We then merged the 1,973 destructor images and 986 annotated images to obtain a map database containing 2,959 images. Fig. 2b presents examples of changing objects in the dataset.

Performance on the ICD task is evaluated in terms of top- $X, Y$  accuracy. First, we estimate an LoC image using an ICD algorithm on the top- $Y$  self-localization hypotheses. We then impose a 2D grid with  $10 \times 10$  pixel sized cells on the query image and estimate an LoC for each cell by max-pooling the pixel-wise LoC values from all pixels that belong to that cell. Next, all cells from all images in the map are sorted in descending order of LoC, and the accuracies of the top- $X$  items in the list are evaluated. We evaluate the top- $X, Y$  accuracy for different  $X$  thresholds in consideration for the intersection-over-union (IoU) criterion [12]. For a specific  $X$  threshold, a successful detection is defined as a changed object whose annotated bounding box is sufficiently covered ( $\text{IoU} \geq 50\% \text{ or } 25\%$ ) by the top- $X$  percent of cells.

TABLE I  
TOP- $X$  ACCURACY FOR AE METHOD [%].

top- $X$	generic				season-specific	
	k=1	k=5	k=10	k=15	k=1	k=10
5%	1.5	1.5	1.0	1.8	1.6	2.3
10%	7.0	7.8	8.1	8.3	8.1	10.3
15%	17.5	18.4	19.3	18.1	17.7	19.6
20%	28.3	31.1	31.6	30.9	29.5	35.1

TABLE II  
BASIC PERFORMANCE (TOP- $X$  ACCURACY [%]).

top- $X$	IoU $\geq$ 50[%]		IoU $\geq$ 25[%]	
	LCD	AE	LCD	AE
5%	6.1	2.0	14.1	6.2
10%	11.1	4.6	27.3	14.4
15%	28.7	7.4	57.5	25.3
20%	47.0	11.6	71.4	38.3

### B. Comparing Methods

We compared the proposed method to a benchmark method, namely AE reconstruction error -based anomaly detection (denoted AE) [18].

The AE method evaluates the LoC at each pixel based on the L2 distance between that pixel and a pixel reconstructed by an AE. Every image is resized to  $128 \times 128$  pixels prior to inputting it to AE. To avoid overfitting, we constructed  $k$  different AEs. First, the reference image set was divided into  $k$  disjoint clusters, and each AE was trained on one cluster. For set division, we employed the k-means clustering algorithm with the number of clusters set to  $k$ . Each trained AE was used as the background model for the reference images belonging to the corresponding cluster.

Table I lists the results of preliminary experiments on the influence of  $k$  on top- $X$  accuracy when assuming the availability of a GT viewpoint. The  $k$  AEs were trained on a single season-generic training set (generic), or four season-specific training sets (season-specific). In the experiments described below, we set  $k=10$  and used the season-generic AEs.

### C. Basic Performance

In the current paper, we focused on the basic performance of the LCD-ICD framework and compared its performance to the benchmark method. To this end, we considered a relatively small map database, and constructed a database with  $N = 100$  images consisting of a GT reference image and  $(N - 1)$  non-GT reference images, which were random samples from the 2,959 total reference images.

We employed an LCD system that represents each image with a size-six BoLF consisting of a full image AE feature and five unsupervised OPR AE features (section II-A). Following our previous work in [14], relative contribution of the NBNN value of each OPR compared to that of the entire image was set 1/20. We set the number of viewpoint hypotheses  $Y$  to 10. This means that for ICD, each query image was compared against 10 different reference images retrieved from the map. Fig. 3 presents the performance results for the self-localization problem.

Table II lists the top- $X, Y$  accuracies of the proposed method (LCD) and the benchmark method. One can see that the performance of the proposed method is much better than that of the AE method.

## VI. CONCLUSIONS

The primary contribution of this paper is the proposal of a novel vSLAM component called LCD-ICD that facilitates simultaneous LCD and ICD. We demonstrated that LCD can be reused as the main processing for ICD with minimal extra cost. We also designed LCD-agnostic strategies for fusing information from multiple local features and aggregating LoC images from different viewpoint hypotheses. The result is a maintenance-free LCD-ICD framework that requires no background modeling or detector engine and is agnostic to the choice of LCD systems.

## REFERENCES

- [1] M. Cummins and P. Newman, "Appearance-only slam at large scale with fab-map 2.0," *The International Journal of Robotics Research*, vol. 30, no. 9, pp. 1100–1123, 2011.
- [2] K. Tanaka, "Cross-season place recognition using nbnn scene descriptor," in *2015 IEEE/RSJ International Conference on Intelligent Robots and Systems (IROS)*. IEEE, 2015, pp. 729–735.
- [3] R. J. Radke, S. Andra, O. Al-Kofahi, and B. Roysam, "Image change detection algorithms: a systematic survey," *IEEE transactions on image processing*, vol. 14, no. 3, pp. 294–307, 2005.
- [4] L. Gueguen and R. Hamid, "Large-scale damage detection using satellite imagery," in *Proceedings of the IEEE Conference on Computer Vision and Pattern Recognition*, 2015, pp. 1321–1328.

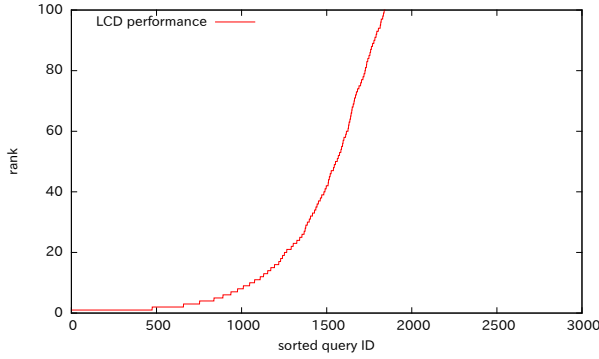


Fig. 3. LCD performance.

- [5] W. Sultani, C. Chen, and M. Shah, "Real-world anomaly detection in surveillance videos," *Center for Research in Computer Vision (CRCV), University of Central Florida (UCF)*, 2018.
- [6] W. Churchill and P. Newman, "Experience-based navigation for long-term localisation," *The International Journal of Robotics Research*, vol. 32, no. 14, pp. 1645–1661, 2013.
- [7] K. Tanaka, "Detection-by-localization: Maintenance-free change object detector," in *Robotics and Automation (ICRA), 2019 IEEE International Conference on*.
- [8] E. Garcia-Fidalgo and A. Ortiz, "ibow-lcd: An appearance-based loop-closure detection approach using incremental bags of binary words," *IEEE Robotics and Automation Letters*, vol. 3, no. 4, pp. 3051–3057, 2018.
- [9] K. Kim, T. H. Chalidabongse, D. Harwood, and L. Davis, "Real-time foreground–background segmentation using codebook model," *Real-time imaging*, vol. 11, no. 3, pp. 172–185, 2005.
- [10] P. Xu, F. Davoine, J.-B. Bordes, H. Zhao, and T. Denœux, "Multimodal information fusion for urban scene understanding," *Machine Vision and Applications*, vol. 27, no. 3, pp. 331–349, 2016.
- [11] N. Carlevaris-Bianco, A. K. Ushani, and R. M. Eustice, "University of michigan north campus long-term vision and lidar dataset," *The International Journal of Robotics Research*, pp. 1023–1035, 2015.
- [12] J. Redmon and A. Farhadi, "YOLO9000: better, faster, stronger," *CoRR*, vol. abs/1612.08242, 2016.
- [13] N. Merrill and G. Huang, "Lightweight unsupervised deep loop closure," in *Proc. of Robotics: Science and Systems (RSS)*, 2018.
- [14] K. Tanaka, "Unsupervised part-based scene modeling for visual robot localization," in *Robotics and Automation (ICRA), 2015 IEEE International Conference on*. IEEE, 2015, pp. 6359–6365.
- [15] A. Mourão, F. Martins, and J. Magalhães, "Multimodal medical information retrieval with unsupervised rank fusion," *Computerized Medical Imaging and Graphics*, vol. 39, pp. 35–45, 2015.
- [16] K. Tanaka, "Self-localization from images with small overlap," in *2016 IEEE/RSJ International Conference on Intelligent Robots and Systems, IROS 2016*, 2016, pp. 4497–4504.
- [17] J. G. Mangelson, D. Dominic, R. M. Eustice, and R. Vasudevan, "Pairwise consistent measurement set maximization for robust multi-robot map merging," in *Proceedings of the IEEE International Conference on Robotics and Automation*, 2018, pp. 1–8.
- [18] M. Sabokrou, M. Fathy, and M. Hoseini, "Video anomaly detection and localisation based on the sparsity and reconstruction error of auto-encoder," *Electronics Letters*, vol. 52, no. 13, pp. 1122–1124, 2016.